Received: 1 December 2023 | Revised: 14 June 2024 | Accepted: 2 July 2024

DOI: 10.1002/rob.22399

RESEARCH ARTICLE

WILEY

Nezha-SeaDart: A tail-sitting fixed-wing vertical takeoff and landing hybrid aerial underwater vehicle

Yufei Jin[1] | Zheng Zeng[1,2] | Lian Lian[1,2]

[1]School of Oceanography, Shanghai Jiao Tong University, Shanghai, China

[2]State Key Laboratory of Ocean Engineering, Shanghai Jiao Tong University, Shanghai, China

Correspondence
Zheng Zeng, School of Oceanography, Shanghai Jiao Tong University, 200240 Shanghai, China.
Email: zheng.zeng@sjtu.edu.cn

Funding information
Science and Technology Commission of Shanghai Municipality Project, Grant/Award Number: 20dz1206600; Natural Science Foundation of Shanghai, Grant/Award Number: 20ZR1424800; Oceanic Interdisciplinary Program of Shanghai Jiao Tong University, Grant/Award Numbers: SL2022ZD106, SL2023ZD206

Abstract

This paper presents the design, manufacturing and testing of a tail-sitting vertically takeoff and landing fixed-wing hybrid aerial underwater vehicle (HAUV) called Nezha-SeaDart. Nezha-SeaDart can vertically take off and land from ground and water, cruise in the air with lift generated by the wings, seamlessly cross the water–air interface and operate underwater like an autonomous underwater vehicle. Nezha-SeaDart underwent a 10-day field test in China's Thousand Islands Lake of Zhejiang Province, proving its ability to perform full cross-domain missions. This research has the following contributions to the field of HAUV. (i) A working prototype of vertical takeoff and landing tail-sitting HAUV with all basic functions verified and full mission cycle capability demonstrated in a field test. (ii) An HAUV that travels fast both in the air and underwater. (iii) An HAUV capable of autonomous and seamless water exit that does not rely on a dedicated propulsion system. (iv) A method of sizing the vehicle's wing and thrust considering aerial cruises, underwater operations, and seamless water exits.

KEYWORDS
hybrid aerial underwater vehicle, rapid transition, robustness, tail-sitter

1 | INTRODUCTION

Hybrid aerial underwater vehicles (HAUVs) possess the ability to travel both in the air and underwater and freely cross the water–air boundary. The development of HAUVs requires integrating the aerial and underwater systems, which are vastly different, into the same platform. Nowadays, most HAUVs are developed based on mature aerial platforms, like, multirotor and fixed-wing unmanned aerial vehicles (UAVs). Aerial platforms are modified and waterproofed to suit underwater environments and usually operate underwater, like, autonomous underwater vehicles (AUVs) (Yao et al., 2023; Zeng et al., 2022).

The Loon Copter developed by Oakland University is a quadcopter HAUV. The vehicle flies like a regular quadcopter in the air. When landing on the water, the vehicle uses a water tank to pitch the vehicle −90° and convert to AUV mode. The vehicle uses the water tank for buoyancy control in AUV mode and four aerial propellers for underwater locomotion and attitude control (Alzu'bi et al., 2018). The Nezha-mini developed by Shanghai Jiao Tong University (SJTU) is a quadcopter HAUV. The vehicle flies like a regular quadcopter in the air. Three underwater propellers control the vehicle during underwater operation (Bi et al., 2022). The same team also developed a heavier quadcopter HAUV, Nezha-IV. It uses four aerial propellers and eight underwater thrusters. Nezha-IV weighs 21 kg, can carry up to 7 kg of payload, and has demonstrated full mission profile capability in a real ocean environment (Jin et al., 2024). Also based on a quadcopter platform, a team from the National University of Singapore developed a morphable quadrotor HAUV that uses thrust vectoring to rotate the propellers for underwater locomotion instead of pitching the whole vehicle or having dedicated underwater propellers (Tan & Chen, 2020).

A team from Beihang University has developed a prototype amphibious aircraft named Flying Fish equipped with folding wings and a ballast water tank. Flying Fish can take off and land on the

water surface in the form of a seaplane, and can also submerge using the ballast water tank to change buoyancy. The prototype has completed testing on lakes, verifying basic underwater navigation, water surface takeoff, airborne flight, and landing capabilities. However, Flying Fish utilizes a water surface takeoff method, which requires a long takeoff distance and is susceptible to disturbances from the water surface (Yao et al., 2014). The EagleRay is a fixed-wing HAUV developed by North Carolina State University. It has a conventional fixed-wing configuration with an extra underwater propeller at its empennage. Its wing is specially designed for fast draining when leaving the water surface. When transitioning from water to air, the vehicle floats at the water's surface with its nose pointing upwards and its aerial propeller above it. The aerial propeller then pulls out the vehicle (Stewart et al., 2018; Weisler et al., 2018). Johns Hopkins University has developed a triangular-wing HAUV made of carbon fiber panels and foam and conducted tests focusing on water-exit operations in a pool. The test results indicate that the water-exit process of this fixed-wing HAUV aircraft imposes strict requirements on the aircraft's attitude. If the attitude and speed during water exit cannot be fully matched, the aircraft will fail to generate sufficient lift and eventually fall back into the water (Moore et al., 2018). The Dipper is another functional fixed-wing HAUV developed by the Swiss Federal Institute of Technology in Zürich. It also has a conventional fixed-wing configuration and a dedicated underwater propeller. Unlike the EagleRay, its wings can sweep backwards to reduce drag when operating underwater. It also used one single motor to power both aerial and underwater propellers. During the water-to-air transition, the vehicle expands its wings at the water's surface, and aerial propellers pull out the vehicle. However, the vehicle cannot perform a jumping dive-out due to the lack of efficient control at the water surface (Rockenbauer et al., 2021). Researchers at the Royal Melbourne Institute of Technology in Australia have also designed a prototype of fixed-wing HAUV with foldable wings. Their studies indicate that the wings of fixed-wing HAUV experience significant resistance during cross-medium transitions and may even be damaged during water entry due to high-speed impact with the water surface. Foldable wings, on the other hand, can enhance the operational efficiency of the aircraft and better protect the relatively fragile wings during cross-medium transitions (Guo, 2019; Guo et al., 2019). Longbow II is another foldable-wing HAUV developed by Harbin Engineering University. The team proved the foldable-wing's effectiveness of drag reduction underwater by pool experiments and demonstrated the vehicle's water-exit capability in a lake test (Sun et al., 2024).

Multirotor HAUVs have inherent flight stability and structure simplicity from multirotor UAVs. With a compact size, they are less affected by the perturbations at the water surface, and the robustness of the control system gives them generally good water-exit stability. However, as all lift in the air is provided by the rotors and the excessive drag created by the non-streamline structures underwater, multirotor HAUVs are not quite efficient in operation. In comparison, fixed-wing HAUVs fly with lift provided by the wings in the air, and the streamlined shape of the vehicle creates less drag when operating underwater. Hence, they are more efficient compared with multirotor HAUVs. However, fixed-wing HAUVs are usually larger than multirotor HAUVs with similar weight and have limited low-speed control authority. As a result, they are subject to more disturbance at the water surface and are less robust during water exits.

To improve the water-exit stability of fixed-wing HAUVs, a team from Imperial College London developed a water jet propulsion system for fast water exits. The water jet is propelled by compressed gas and can produce stable and consistent thrust throughout the water-exit phase (Siddall & Kovac, 2015). The system is later applied to their HAUV, the aquatic micro aerial vehicle, and proven effective (Sareh et al., 2017; Siddall et al., 2017). They also developed another vehicle that uses solid explosives instead of compressed gas to propel the water jet (Siddall et al., 2018; Zufferey et al., 2019). However, as neither the compressed gas nor explosives can be resupplied during operation, these vehicles can only exit water once each mission. The same team also developed a gearbox system that that can engage different gearing ratios based on the direction of the drive shaft, without the need for additional actuators. With a variable gearing ratio, the propulsion system can adapt to the working substance change during a cross-domain mission and maintain good efficiency both in air and underwater (Tan et al., 2017).

Trying to combine the advantages of fix-wing and multirotor HAUVs, a team from SJTU finds the balance between efficiency and cross-domain stability by combining underwater gliders (UGs) with vertical takeoff and landing (VTOL) fixed-wing UAVs. Under this principle, they developed the Nezha series, including conventional VTOL versions (Lyu et al., 2022) and tail-sitting VTOL versions (Lu et al., 2018, 2019, 2021). The vehicles demonstrated good water-exit stability and had better operation efficiency than multirotor HAUVs, especially when operating underwater in UG mode. Despite the combination of fixed-wing UAV and UG utilized the wing in both modes. The vehicles require a rather heavy buoyancy control system for underwater operations. Hence, they have to be built relatively heavier, affecting the vehicles' overall efficiency, and none of them has demonstrated their fixed-wing cruise capability in field tests (Figure 1).

To better integrate the advantages of fixed-wing and multirotor HAUVs, as well as, improving water-exit stability, we designed a tail-sitting VTOL fixed-wing HAUV named Nezha-SeaDart. The configuration was selected due to the following characteristics. (i) Acceptable efficiency in both air and underwater. (ii) Sufficient low-speed control authority for water exit. (iii) Robust structure to survive unstable environments. This paper will present the vehicle's design, fabrication, and testing. Nezha-SeaDart operates like a quadcopter during vertical takeoff and water-to-air transit for better stability and robustness. It flies with lift generated by a pair of delta panel wings during aerial cruises and maneuvers automatically like an AUV when operating underwater. Four brushless motors provide thrust both in the air and underwater and control the vehicle's yaw with differential thrust. In addition, a pair of elevons mounted at the trailing edge of the wings control the vehicle's pitch and roll. Nezha-SeaDart weighs

FIGURE 1 Nezha-SeaDart at the Thousand Islands Lake.

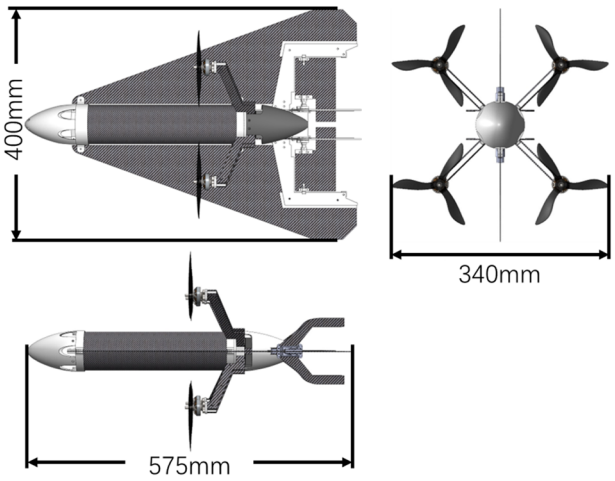

FIGURE 2 Three-views of Nezha-SeaDart.

1500 g in total with a length of 525 mm and a wingspan of 400 mm, as shown in Figure 2. Its four brushless motors mounted with 5.1-in. propellers can produce 36 N thrust in the air. We manufactured two testing vehicles of Nezha-SeaDart and underwent 10 days of testing in the Thousand Islands Lake in Zhejiang Province of China. During the test, the vehicles demonstrated the ability to take off vertically from both water and land, cruise in the air with lift produced by the wings, plunge-dive into the water, seamless water exit and operate autonomously underwater.

This research brings several significant contributions to the field of HAUV. (i) A functional prototype of a VTOL tail-sitting HAUV has been developed, with all essential functions confirmed and its ability to complete full mission cycles demonstrated during a field test. (ii) The HAUV designed in this research showcases rapid travel capabilities both in aerial and underwater environments. (iii) The HAUV developed is capable of autonomously transitioning from underwater to water exit without the need for a dedicated propulsion system, ensuring seamless operation. (iv) This research introduces a novel approach to sizing the vehicle's wing and thrust, taking into account requirements for aerial cruising, underwater operations, and seamless transitions between water and air.

2 | CONFIGURATION SELECTION AND VEHICLE DESIGN

2.1 | Configuration selection

To systematically select the best configuration that fits our goal of designing an efficient, agile, and robust HAUV, we designed a multicriterial analysis to evaluate the possible configurations in the following aspects: Weight, aerial mobility, underwater mobility, aerial efficiency, underwater efficiency, water-to-air transit, durability, easiness of manufacturing, and technology readiness level (TRL). A scaling factor of 2 is given to weight, aerial mobility, underwater mobility, air-to-water transit, and TRL, for they have more impact on the research's objective. Cruise efficiency, underwater efficiency, durability, and easiness of manufacturing are also relevant criteria but not as important. Hence, they are given a scaling factor of 1. The aerial platform will be selected from a Fixed-wing tail-sitter, Multi-rotor, Tiltrotor, Conventional VTOL fixed-wing, and Coaxial dual-rotor helicopter. Modes of underwater locomotion will be chosen from AUV using aerial propellers, AUV using dedicated underwater thruster, UG, AUV using the soft morphing structure and Legged. The following options are listed for selection for buoyancy control: uncontrolled, variable buoyancy system using piston or bladder, and vertical thruster. Configurations that are more commonly used in the

area are selected as the datum and given a score of 1. If considered to be better than the datum, other configurations will be scored 2, 1 if similar, and 0 if worse. HAUVs are a new vehicle type with only a few functional prototypes, and the relevant historical data are very limited. Therefore, the result of this analysis is empirical and subject to our experience and understanding of the topic and is not entirely objective. It only represents our decision-making process instead of quantitative comparison.

Based on the result of the multicriterion analysis, as shown in Table 1, the best configuration that suits our goal is a tail-sitter VTOL fixed-wing HAUV without active buoyancy control and uses aerial motors and propellers for both aerial and underwater operations. The selected configuration is then compared with existing configurations using the same multicriterion analysis structure.

The result in Table 2 shows that the selected configuration wins over other configurations for being lightweight, agile both in air and underwater, and robust during the water-to-air transit.

2.2 | Mission profile

The target mission profile of the vehicle is shown in Figure 3. First, the vehicle takes off vertically in quadcopter mode from land or water. Then it pitches down 90° and converts to fixed-wing mode. In fixed-wing mode, the vehicle flies with the lift generated by the wings at a velocity much higher than regular quadcopters. Next, the vehicle pitches down and dives into the water surface with propellers switched off on arrival at the mission area. The vehicle then switches to underwater mode and completes the preset underwater mission. After finishing the underwater mission, the vehicle returns to the water surface with a nose-up attitude and takes off vertically. Then the vehicle flies toward the landing field, a designated land or water area, and lands vertically.

2.3 | Vehicle design

One of the most significant challenges in designing a fixed-wing HAUV is finding the balance between lift, buoyancy and weight of the vehicle. The center of buoyancy (CoB) needs to be slightly in front of the center of gravity (CoG) to give the vehicle a nose-up attitude at the water surface for vertical takeoff. The vehicle's aerodynamic center (AC) needs to be close enough to the CoG to acquire the necessary flight stability. In addition, the plunge dive phase requires the vehicle's wings and motor arms to be strong enough to withstand the impact. As there is no active buoyancy control on the vehicle, the buoyancy needs to be slightly larger than the weight to ensure the vehicle floats, at the same time, is not too large that the vehicle's controls cannot compensate. This prevents using foam-cored wings or sandwiched load-bearing structures, which have excellent properties but add too much to the buoyancy.

Certain compromises were made when designing the vehicle to balance these contradicting criteria. We designed a pair of delta panel wings for the vehicle. It meets the requirements by having a small volume, small impact area when hitting water surface and relatively rearwards AC. However, the delta panel wing has a lower maximum lift coefficient and lift-to-drag ratio than traditional rectangular wings with aerofoil cross-sections. Hence the vehicle needs to fly faster in the air and does not have the best aerodynamic efficiencies. The motor arms of the vehicle are arranged in an "X" shape viewing from the front. The motor arms are made of two pieces of vertically oriented carbon fiber reinforced plastic plates spaced by nylon spacers to achieve good strength and stiffness in both lateral and longitudinal directions without adding too much buoyancy to the vehicle. However, such a design creates additional drag during the fixed-wing cruise. Four motors are placed 100 mm away from the x-axis of the vehicle and 75 mm away from adjacent motors. A pair of elevons actuated by waterproofed servos are designed to control the vehicle's pitch and roll instead of using the differential thrust of the motors. It maintains the vehicle's attitude control in the plunge dive phase, during which the motors will be switched off to avoid current spikes when hitting the water surface. Figure 4 shows the external components and dynamic centers of Nezha-SeaDart.

The vehicle's electrics and batteries are placed in a pressure vessel made of carbon fiber tube. The front end of the pressure vessel is permanently sealed with a nylon cap and high-strength epoxy resin. The rear end of the pressure vessel is sealed with O-rings pressed against the inner wall by a nylon insert. Electronics and batteries are mounted on the nylon insert using carbon fiber plates and aluminum columns, as shown in Figure 5. In need of access, components inside the pressure vessel can be pulled out together with the nylon insert. The electric speed controller (ESC) that controls the four brushless motors is sealed with epoxy resin and placed outside the pressure vessel for better heat dissipation. Wings are directly connected to the carbon fiber tube for longitudinal stiffness. All other parts are connected to the nylon insert so that removing the pressure vessel does not affect the structure and electrical connections between the components. The vehicle's frame passed a pressure test in lab environments. All components remained functional at a depth of 50 m underwater with no visible damage or leakage.

3 | SIZING OF WINGS AND PROPULSION SYSTEM

In designing an ordinary aircraft, the wing's size and AC should be roughly decided in the initial design phase. However, in designing a VTOL tail-sitting HAUV, we found it difficult to follow the ordinary procedure due to the lack of relevant theory and historical data. Therefore, we decided to design the vehicle's wing after manufacturing the rest. By doing so, we significantly reduced the number of variables that need to be considered, and the analysis can be less complex and less dependent on historical data. The manufactured vehicle frame without the wings has a mass of 1.37 kg and produces 13.2 N of buoyance. The CoM is 290 mm behind the nose, and the

TABLE 1 System-level multicriteria analysis.

Configuration	Criterions	Weight	Cruise mobility	Underwater mobility	Cruise efficiency	Underwater efficiency	Water to air	Durability	Manufacturing	TRL	Total
	Scaling factor	2	2	2	1	1	2	1	1	2	
Aerial platform	Fixed-wing tailsitter	1	2	2	2	2	1	1	1	1	20
	Multicopter	1	1	1	1	1	1	1	1	1	14
	Tiltrotor	0	2	2	2	2	1	0	0	0	14
	Conventional VTOL fixed wing	0	2	1	2	1	0	0	0	1	11
	Coaxial dual-rotor helicopter	2	1	0	1	0	1	0	0	0	9
Underwater locomotion	Aerial propeller	2	1	0	2	0	1	2	2	1	16
	Dedicated underwater thruster	1	1	1	1	1	1	1	1	1	14
	Underwater glider	0	1	0	1	2	1	0	2	1	11
	Soft morphing structure	1	1	0	1	1	1	0	0	0	8
	Legged	0	1	0	1	1	1	0	0	0	6
Buoyancy control	Uncontrolled	2	1	1	1	0	1	2	2	1	17
	Piston VBS	1	1	1	1	1	1	1	1	1	14
	Compressed air	1	1	1	1	1	1	1	1	1	14
	Bladder VBS	0	1	1	1	1	1	1	1	1	12
	Vertical thruster	2	1	1	1	0	1	1	1	1	15
		Selected configuration						Datum configuration			

Abbreviations: TRL, technology readiness level; VBS, variable buoyancy system; VTOL, vertical takeoff and landing.

TABLE 2 Vehicle level multicriteria analysis.

Configuration	Criterions	Weight	Cruise mobility	Underwater mobility	Cruise efficiency	Underwater efficiency	Water to air	Durability	Manufac-turing	TRL	Total
	Scaling factor	2	2	2	1	1	2	1	1	2	
Vehicle concepts	Tailsitter fixed-wing without active buoyancy control and uses aerial motors and propellers underwater	2	2	1	2	1	1	1	1	1	19
	Multirotor with dedicated underwater thruster and vertical thruster for buoyancy control	1	1	1	1	1	1	1	1	1	14
	Tailsitter fixed-wing underwater glider with pressured air buoyancy control	0	2	0	2	2	1	0	0	1	12
	Conventional VTOL fixed-wing underwater glider with Piston VBS	0	2	0	2	2	1	0	0	1	12
	Fix-wing with dedicated underwater propeller and no active buoyancy control	2	2	1	2	1	0	1	1	1	17
						Selected configuration			Datum configuration		

Abbreviations: TRL, technology readiness level; VBS, variable buoyancy system; VTOL, vertical takeoff and landing.

CoB is 263 mm behind the nose. Fuselage has a length of 490 mm and a diameter of 68 mm. We used Young's method to estimate the parasitic drag of the frame and calculated the form drag, assuming it is a streamlined body with four rectangular cross-section struts.

3.1 | Drag estimation

3.1.1 | Parasitic drag

Young's method estimates the friction drag coefficient for a section with mixed laminate and turbulent flow using the following:

$$C_{friction\_mix} = \frac{0.074}{R_e^{0.2}}\left(1 - \left(\frac{x_{tr} - x_0}{c}\right)\right)^{0.8}, \tag{1}$$

where x_0 is the distance from the leading edge to the start point of the fictitious turbulent boundary layer, which can be calculated using

$$\left(\frac{x_0}{c}\right) = 36.9 \times \left(\frac{x_{tr}}{c}\right)^{0.625}\left(\frac{1}{Re}\right)^{0.375}, \tag{2}$$

where Re is the Reynolds number, and x_{tr} is the distance from the leading edge to the turbulent transition point, which is assumed to be at where $Re = 10^5$, hence

$$Re = \frac{vl}{v} = \frac{vx_{tr}}{v} = 10^5, \tag{3}$$

$$x_{tr} = 10^5\frac{v}{v}. \tag{4}$$

The formula can be rearranged to

$$C_{friction\_mix} = \frac{0.074}{\left(\frac{vl}{v}\right)^{0.2}}\left\{1 - \frac{10^5\left[\frac{v}{v} - 36.9*\left(\frac{v}{v}\right)^{1.375}\right]}{l}\right\}^{0.8}, \tag{5}$$

where

v is the freestream velocity.

v is the kinematic viscosity, we used values $1.5e^{-5}$ m^2/s for air and $9.8e^{-7}$ m^2/s for water (20°C, 1 atm).

l is the characteristic length of the structure, in our case, the length of the fuselage, chord length of the wing, and motor arm dimension in the x-direction.

Considering the possibility that, at low-velocity operation, the laminar flow may dominate in some sections. The friction coefficient for full laminate flow is added to the calculation.

$$C_{friction\_lam} = \frac{1.320}{\sqrt{Re}} = \frac{1.320}{\sqrt{\frac{vl}{v}}}. \tag{6}$$

The larger value of $C_{friction\_mix}$ and $C_{friction\_lam}$ is used as the friction coefficient $C_{friction}$.

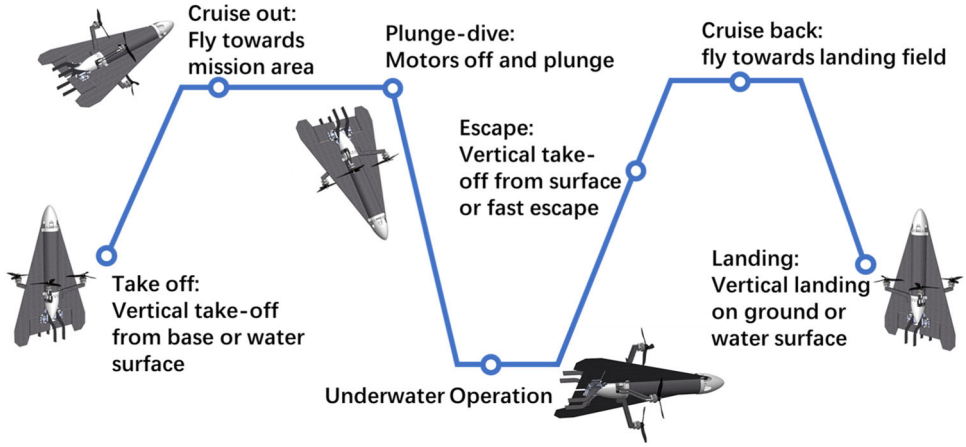

FIGURE 3 Mission profile of tail-sitting fixed-wing hybrid aerial underwater vehicle.

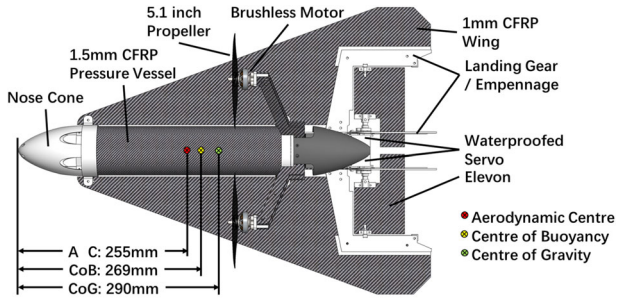

FIGURE 4 External components and dynamic centers of Nezha-SeaDart. CFRP, carbon fiber reinforced plastic; CoB, center of buoyancy; CoG, center of gravity.

Due to the tapering of the wings, the average of $C_{friction}$ for the tip and root chords is used as the friction coefficient of the wings $C_{friction\_wings}$. As this method does not consider the sweep angle of the wings, the wings' geometry is defined with aspect and tapering ratios only. However, analysis shows that changing the aspect and tapering ratios has limited impacts on the parasitic drag. The estimated parasitic drag is strongly correlated to wing area and freestream velocity.

3.1.2 | Form drag

Form drag coefficient of the fuselage $C_{form\_fuselage}$ is assumed to be 0.05 for being a streamlined body with smooth skin. Form drag coefficient of the motor arms C_{form_arm} can be assumed to be 0.8 for having a rectangular cross-section. Cross-sectional areas are used as reference areas. Form drag for the wings is ignored as the wing is a thin plate.

3.1.3 | Lift-induced drag

The wing is considered a low aspect ratio trapezoid plate with a large sweep angle and low tapering ratio. Induced drag is estimated using drag polar:

$$C_d = C_{d0} + \frac{C_l^2}{\pi e AR}. \tag{7}$$

With Oswald efficiency e estimated using Raymer's equation:

$$e = 4.61(1 - 0.045AR^{0.68})(\cos \Lambda_{LE})^{0.15} - 3.1, \tag{8}$$

where

C_{d0} is the zero-lift drag coefficient of the wing, in our case, the parasitic drag.

C_l is the lift coefficient.

AR is the aspect ratio of the wing.

Λ_{LE} is the leading edge sweep angle of the wings.

3.2 | Constrain analysis

A constrain analysis diagram is plotted using power-to-weight ratio P/W and wing loading W/S, as shown in Figure 6. Three working conditions were considered.

(i) *Underwater horizontal cruise*: In this case, the net buoyancy and moment that needs to be balanced can be assumed negligible compared with the vehicle's parasitic drag and form drag. Velocities of 1, 3, and 5 m/s were selected to create three lines in the P/W–W/S diagram (blue lines), governed by the following equation:

$$\frac{P}{W} = \frac{DvS}{W^2} * \frac{W}{S}, \tag{9}$$

where D is the drag estimated using the method mentioned in Section 3.1.

(ii) *Fixed-wing cruise in air*: In this case, the P/W–W/S diagram can be produced using the constrain analysis formula:

$$\frac{P}{W} = \left[qC_{D0}\left(\frac{W}{S}\right)^{-1} + \frac{1}{\pi e AR}\left(\frac{1}{q}\right)\left(\frac{W}{S}\right)\right] * v, \tag{10}$$

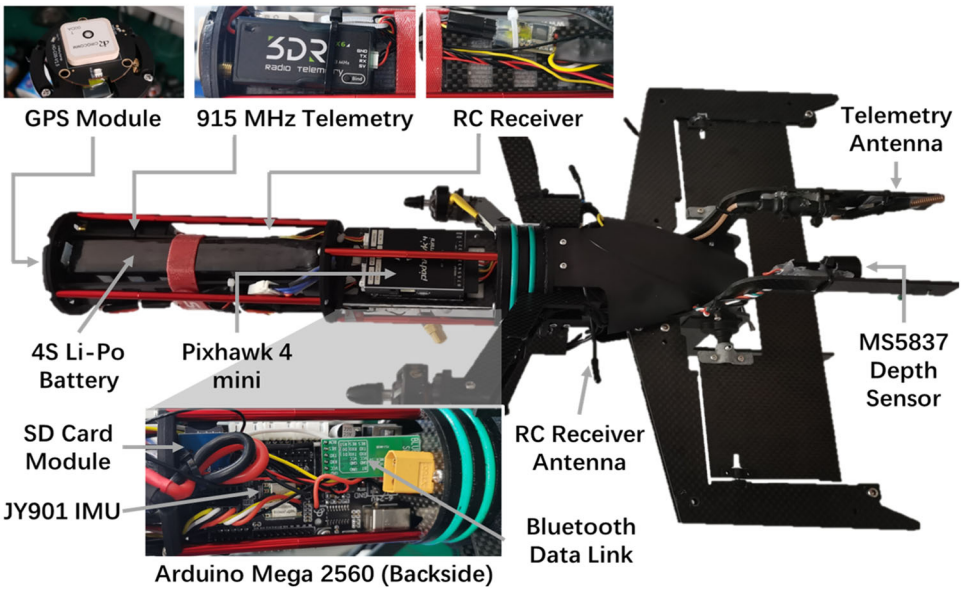

FIGURE 5 Electronics cabin of Nezha-SeaDart. GPC, Global Positioning System; IMU, inertial measurement unit; RC, remote control; SD, secure digital.

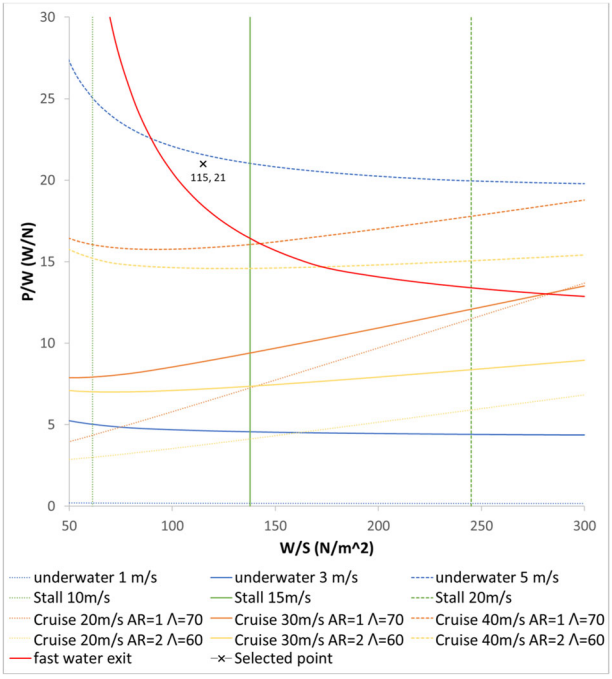

FIGURE 6 Constrain analysis.

where C_{D0} is the zero-lift drag coefficient of the vehicle and q is the dynamic pressure.

Two wing geometries $AR = 2$ $\Lambda_{LE} = 60$ (orange lines) and $AR = 1$ $\Lambda_{LE} = 70$ (yellow lines), are selected to create six lines in the P/W–W/S diagram for velocities 20, 30, and 40 m/s.

When transferring between VTOL and fixed-wing cruise, the vehicle needs to pitch up and down 90° and experiences stall during the process. It is necessary to make sure that the stall speed is acceptable. Lines for three different stall speeds are plotted using the following equation (green lines).

$$\frac{W}{S} = qC_{l\_\max}, \tag{11}$$

where maximum lift coefficient $C_{l\_\max}$ is assumed to be 1.

(iii) *Underwater vertical ascent*: The vehicle must gain sufficient velocity during this phase to jump out of the water surface. When crossing the water surface, thrust is assumed to be zero, and buoyancy and water drag are assumed to be proportional to submerged vehicle length. Air drag is neglected. A Generalized Reduced Gradient algorithm was used to find the velocity and thrust needed during the vertical ascent maneuver for a range of wing areas and created a line in the P/W–W/S diagram (red line).

The P/W–W/S diagram shows that, in general, the vehicle prefers a smaller wing for underwater operation and water-to-air transition. To an extent, a larger wing with a higher aspect ratio and lower sweep gives better aerial cruise efficiency. This result agrees with the general knowledge of AUVs and fixed-wing UAVs. It can be noticed that the previous analysis does not provide sufficient arguments to make a definite decision on the design point. The diagram only tells the range of feasible design points at this stage, more research is needed before it can help making optimization decisions. Our selected design point is $P/W = 21$ W/N and $W/S = 115$ N/m^2, which results in a wing area of 0.128 m^2 and a propulsion power of 294 W. The diagram shows that, such a design will have a maximum aerial cruise velocity higher than 40 m/s, a maximum underwater cruise velocity slightly lower than 5 m/s. The vehicle should have enough power to exit water and have a stall velocity lower than 15 m/s but higher than 10 m/s. When operating underwater, propulsion systems

designed for aerial operation will be inefficient. An overall energy efficiency of 0.3 is assumed. The 30% of the propulsion power will be reserved for attitude control. An increment of another 10% is given to account for miscellaneous drag, including drags created by using control surfaces to balance the vehicle. The design point requested a propulsion system with an input power of 1540 W. We selected a motor, battery and propeller combination with a maximum power of 1747 W. It gives 11.8% excessive power as a safety margin. The wing is designed to be a delta wing with an aspect ratio of 1.26 and a leading edge sweep angle of 68° so that the panel wing will not be too flexible in the air and has a nice impact angle when entering the water. A free fall experiment was conducted to make sure the structure would not break during a water impact. Quantitative analysis of water impact during the water-entry phase is not included in the design loop.

The final design weighs 1500 g and produces 1550 g of buoyancy in fresh water. As shown in Figure 4, CoG is 290 mm behind the nose. AC is 255 mm behind the nose (45 mm in front of CoG). As the vehicle does not have a horizontal stabilizer, its neutral point overlaps with its AC. This means the vehicle is statically unstable in the longitudinal direction. As a result, the vehicle will be more agile in the air. However, it will be difficult to fly without the continuous stabilization of a flight controller. CoB is 269 mm behind the nose (21 mm in front of CoG) and produces 0.32 Nm of torque when fully submerged in fresh water with a horizontal orientation. It is sufficient to give the vehicle a stable nose-up attitude when floating on the water's surface. The differential thrust of the motors or deflection of the elevons during underwater operation can easily compensate for it. With a wing area of 0.128 m^2, the vehicle has a minimum aerial cruise speed of 13 m/s and can reach up to 40 m/s in theory. The most economy cruise velocity is estimated to be 25 m/s, with a lift-to-drag (L/D) ratio of 4.18. Maximum underwater velocity is estimated to be 5 m/s. The vertical velocity needed for a fast water exit is estimated to be 4.77 m/s. Aerial cruise and underwater operation efficiency are also estimated using the same formulas and compared with test data in Section 5.5.

4 | ELECTRONICS AND CONTROL

4.1 | Electronics

Figure 7 shows the electronic design of the vehicle. The vehicle uses a Pixhawk to control its attitude and motion both in the air and underwater. It uses an Arduino as the mission computer to store mission plans and enable automated mission execution. Pixhawk runs a closed-loop control algorithm based on PX4 open-source firmware. Including them in the development significantly shortens the development cycle. By actuating the four brushless motors and two elevons, the Pixhawk can control the vehicle's attitude in both air and underwater and the vehicle's altitude and position in the air while connected to a global positioning system (GPS). A 16-channel RC receiver is connected to the Arduino to receive commands from the remote controller. A depth sensor provides depth information, and an inertial measurement unit (IMU) provides the acceleration, angular velocity, attitude, and heading information to the Arduino. The vehicle carries 48.84 Wh of energy in its 3300 mAh 4 S lithium-polymer battery. The battery supplies 14.8 V main power to the Arduino and the four-in-one ESC. The Arduino has a built-in DC–DC converter that converts the main power supply to 5 V with its built-in step-down converter and supplies it to the Pixhawk. Servos and other electronics get their 5 V power supply from either the Arduino or the Pixhawk, depending on which board they are connected to.

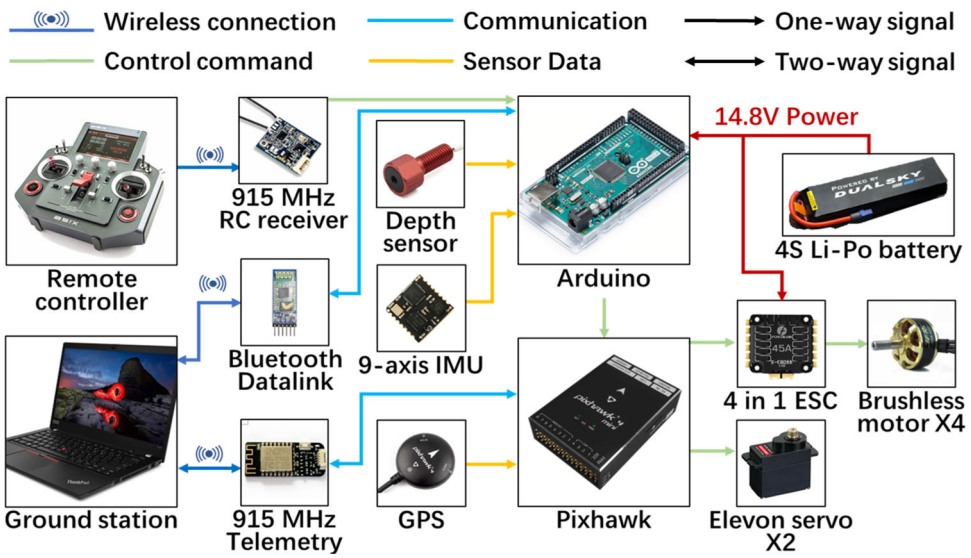

FIGURE 7 Electronic design of Nezha-SeaDart. GPC, Global Positioning System; IMU, inertial measurement unit; RC, remote control.

4.2 | Control

In the air, the vehicle can be controlled using a remote controller. Arduino receives the control signal from the RC receiver and passes the control signal directly to the Pixhawk. With the GPS module enabled, Pixhawk can control the vehicle's position, horizontal drifting speed and altitude in VTOL mode and heading, airspeed and altitude in fixed-wing mode. One of the RC receiver channels is mapped as the switch to underwater operation. When the switch is flipped, Arduino ignores the input from the rest of the channels and calculates commands to be sent to the Pixhawk based on the mission plan uploaded. The Pixhawk controls the vehicle's attitude, using closed-loop proportion and integration and differentiation (PID) control with feedback from its onboard IMU. The Arduino controls the vehicle's depth by sending pitch control commands to the Pixhawk and controls the vehicle's heading by sending yaw control commands to the Pixhawk. The depth and heading data are acquired from the depth sensor and IMU connected to the Arduino.

TABLE 3 Velocity, endurance, and range.

	Velocity (m/s)	Power (W)	Endurance (min)	Range (km)
Aerial cruise	35.2	705.3	4.15	8.76
	24.7	397.7	7.37	10.91
	16.0	431.3	6.79	6.52
	12.6	533.9	5.49	4.13
Hover	0	385.4	7.60	0
Underwater operation	3.0	436.7	6.71	1.20
	1.0	136.3	21.50	1.28

5 | TESTING AND MISSION DEMONSTRATION

In September 2022, we brought the Nezha-SeaDart to the Thousand Islands Lake in Zhejiang Province of China for 10 days of testing. During the test, we verified the vehicle's ability to operate in the air and underwater and automatically transition between air and underwater in relatively calm weather. During the test, the vehicle reached a maximum underwater velocity of 3 m/s (5.8 knots), a maximum VTOL climb rate of 18 m/s and a maximum aerial cruise speed of 35 m/s (126 km/h or 68 knots). Table 3 contains the vehicle's velocity, endurance and range data extracted from the test log. The vehicle has superior velocity and range compared with similar-sized multicopters but is worse than fixed-wing HAUVs.

5.1 | Ground VTOL

During ground vertical takeoff, the vehicle first stands on the platform on its empennage, with its nose pointing vertically upwards. Motors are then powered up and lift the vehicle off the ground. The vehicle's attitude is stabilized using the differential thrust of the four rotors. The two elevons are locked in the neutral position, not used for control in VTOL mode. The GPS acquires location and altitude information for the Pixhawk, and the Pixhawk uses the information to control the vehicle's attitude and thrust to hold the vehicle's location and altitude. The vehicle can slowly gain altitude and move from the platform to a safe fixed-wing transition location. During the vertical landing, the vehicle is controlled by the same logic and lands on the platform. One of the test flights is shown in Figure 8.

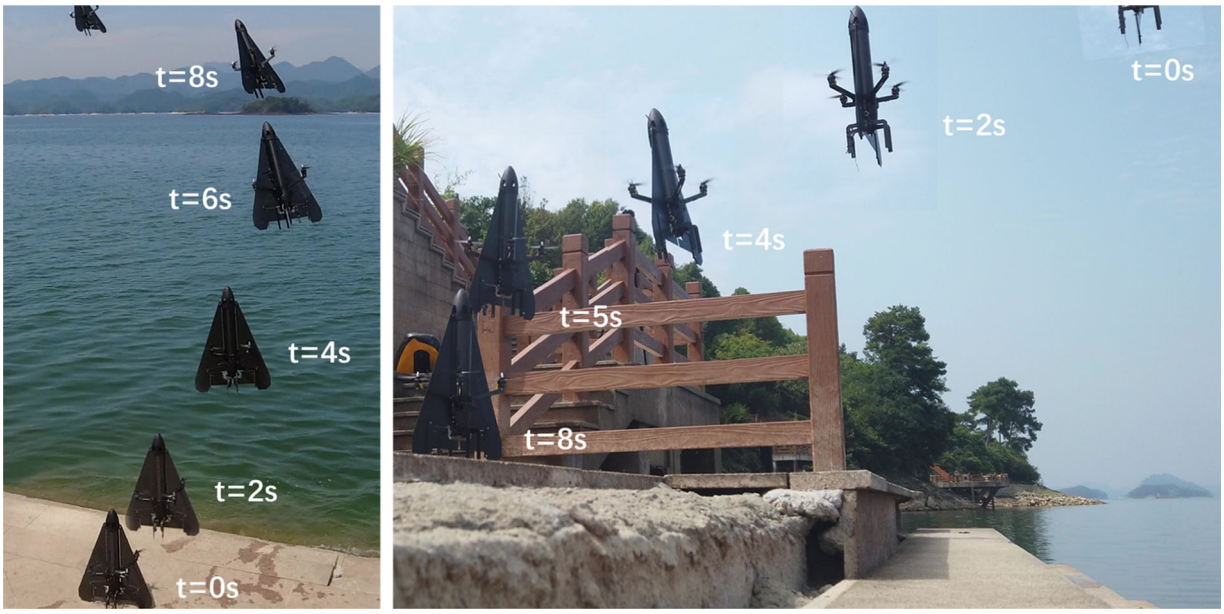

FIGURE 8 (Left) Ground vertical takeoff and (Right) ground vertical landing.

5.2 | Water takeoff and landing

When floating freely on the water's surface, the vehicle has a vertically nose-up attitude. The motors will be powered up in quadcopter mode to take off from the water. Thrust they create lifts most of the vehicle out of the surface with propellers operating on the water's surface. Once the vehicle's attitude is stabilized, the throttle is increased further to bring the vehicle into the air. To land on the water surface, the vehicle slowly approaches the water surface in quadcopter mode. The motors are switched off when the vehicle is near the water's surface. One of the test flights is shown in Figure 9.

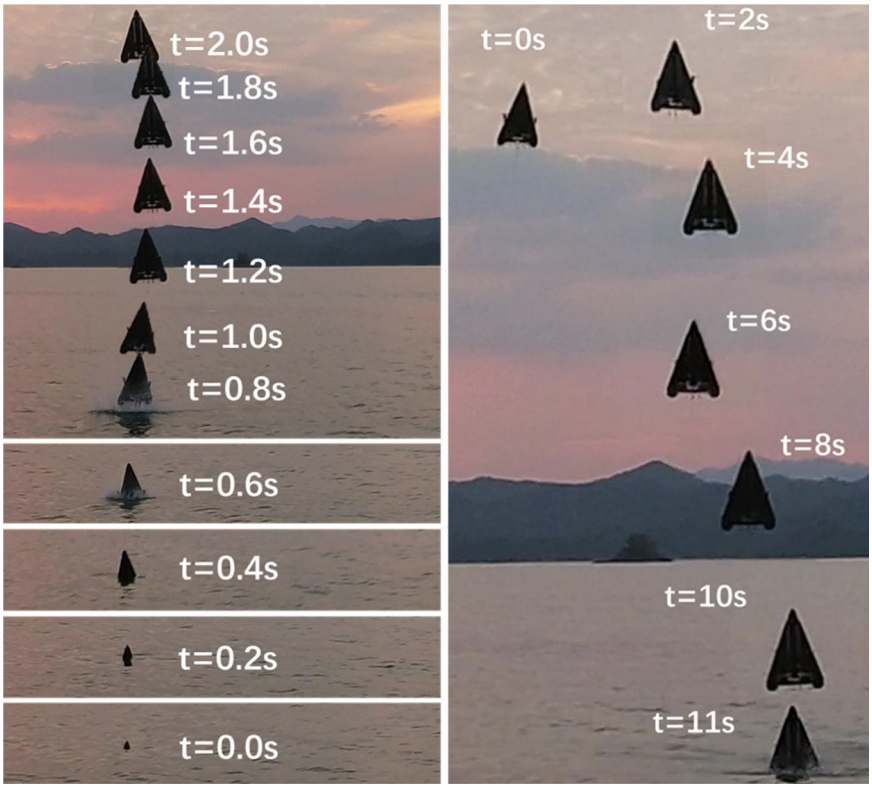

FIGURE 9 (Left) Water vertical takeoff and (Right) water vertical landing.

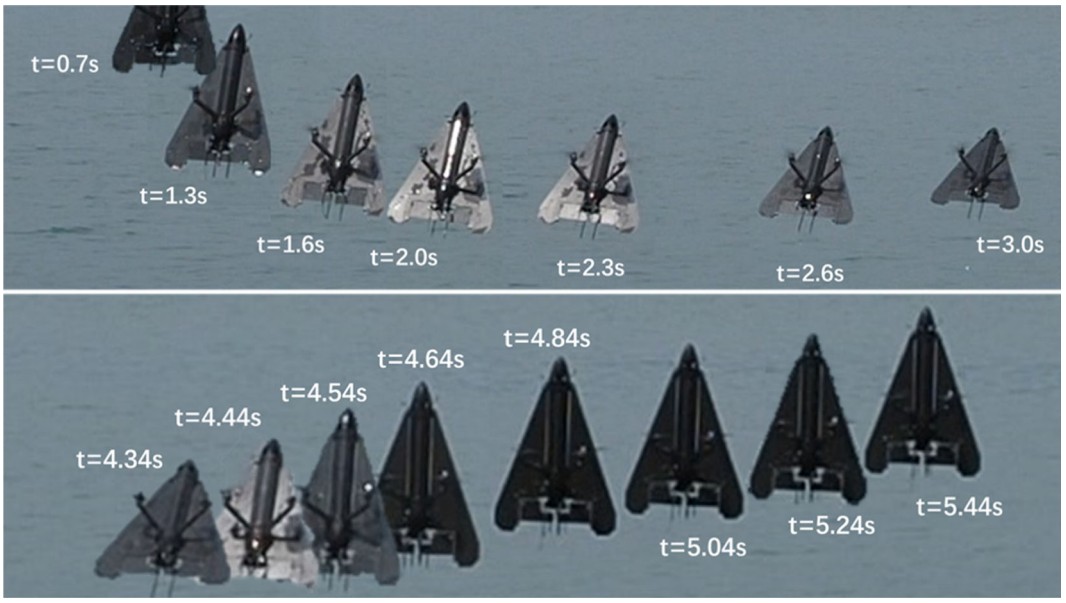

FIGURE 10 (Top) VTOL to cruise transit and (Bottom) cruise to VTOL transit. VTOL, vertical takeoff and landing.

5.3 | Transition between VTOL and cruise

The vehicle is first controlled to a safe altitude and location in quadcopter mode. Then the controller activates its two elevons and slowly pitches the vehicle down to the cruise attitude. To transit from fixed-wing flying to VTOL, the vehicle first rapidly pitches up and points the thrust upwards. Then, the vehicle hovers at the current location and altitude in VTOL mode. One of the test flights is shown in Figure 10.

5.4 | Fixed-wing flight and underwater operation

During the fixed-wing flight, the elevons control the vehicle's pitch and roll, and the vehicle's yaw is controlled by differential thrust, as no rudder is installed. With the location and altitude information from the GPS module, the Pixhawk can maintain the vehicle's course and altitude by controlling the vehicle's attitude and thrust. In underwater operation, the vehicle is controlled using the same logic. There is no GPS signal underwater, so the vehicle's location information cannot be acquired. The underwater mission is programmed in terms of the vehicle's desired attitude and the period of holding this attitude. One of the test flights is shown in Figure 11.

To analyze the vehicle's aerial cruise and underwater operation efficiency, four aerial data points and two underwater data points were extracted from the vehicle's log. In Figure 12, the test data are compared with our estimation using formulas stated in Section 3. The estimation and test data follow similar trends. However, the estimated power is generally lower than the test data. This can be due to underestimated drag efficiencies and overestimated propulsion efficiency.

5.5 | Fast water exit and entry

The vehicle can enter and exit the water surface without lingering on the water surface. During the fast water exit, the vehicle is first commanded to reach sufficient depth and pitch up with its nose pointing vertically upwards. The vehicle then speeds and breaks the water's surface. The momentum built-up will be sufficient to bring the propellers off the water. The propellers can then pick up speed and lift the rest of the vehicle off the water's surface. To perform a fast water entry, the vehicle pitches down with its nose pointing vertically downwards and dive with gravity. Propellers are stopped to avoid current spikes while hitting the water surface. The vehicle's attitude is stabilized with elevons. One of the test flights is shown in Figure 13.

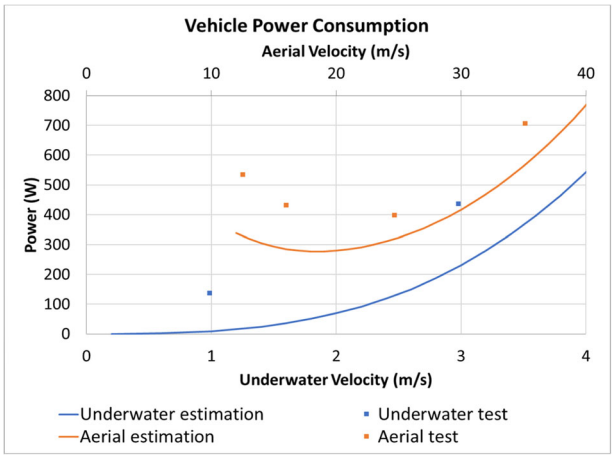

FIGURE 12 Vehicle power consumption.

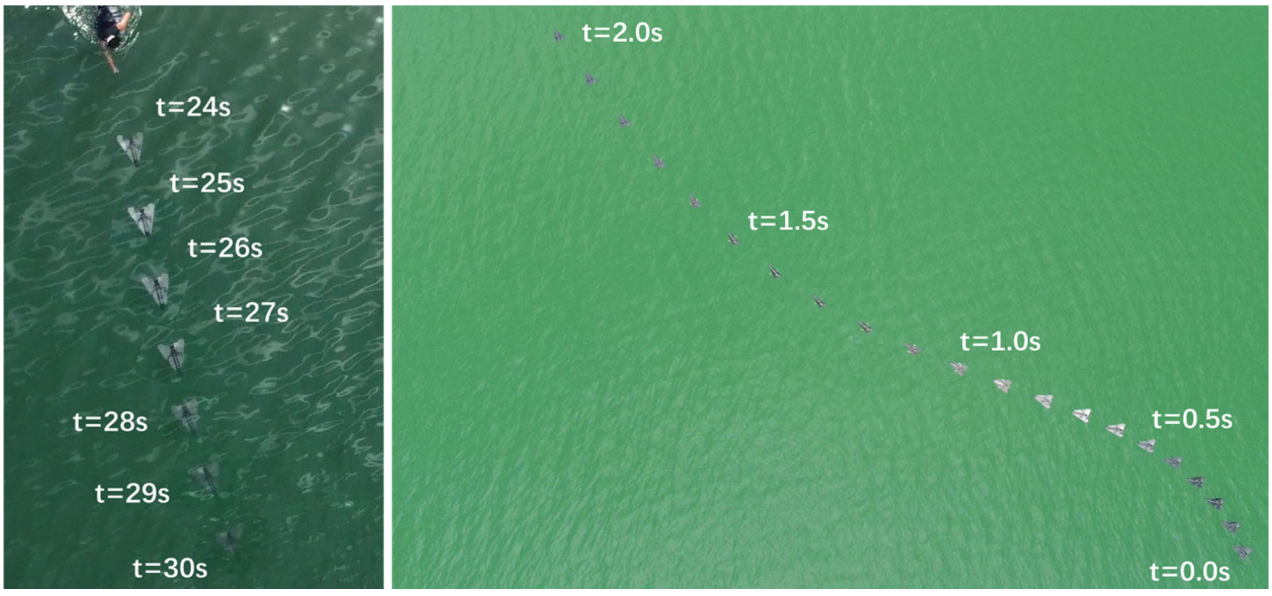

FIGURE 11 (Left) Underwater operation and (Right) fixed-wing cruise.

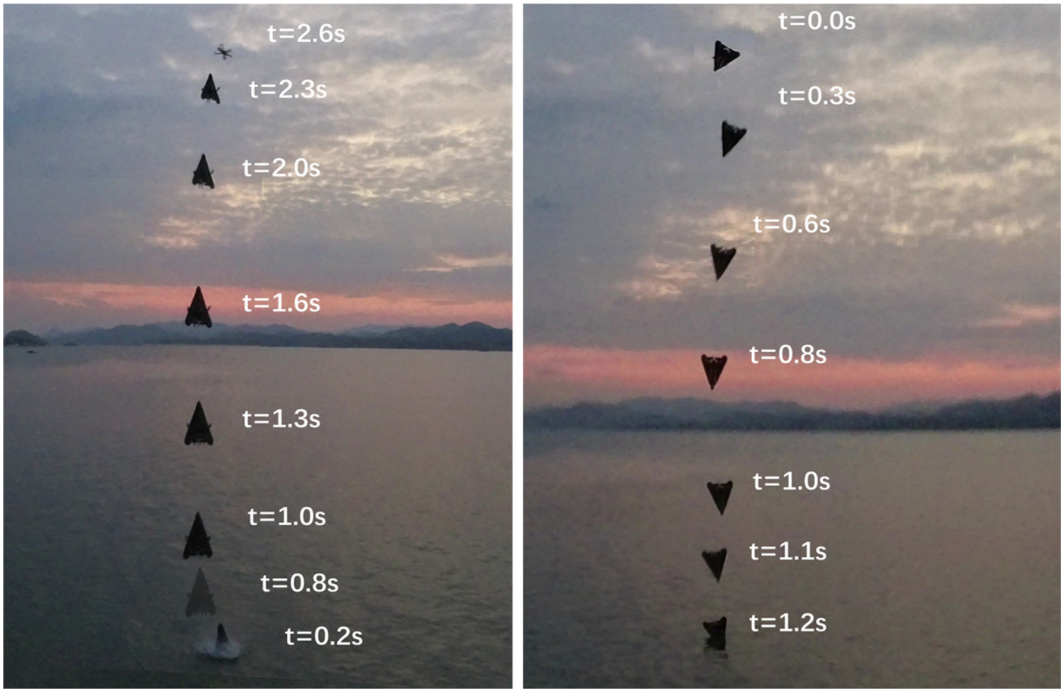

FIGURE 13 (Left) Fast water exit and (Right) fast water entry.

FIGURE 14 Breakdown of fast water exit.

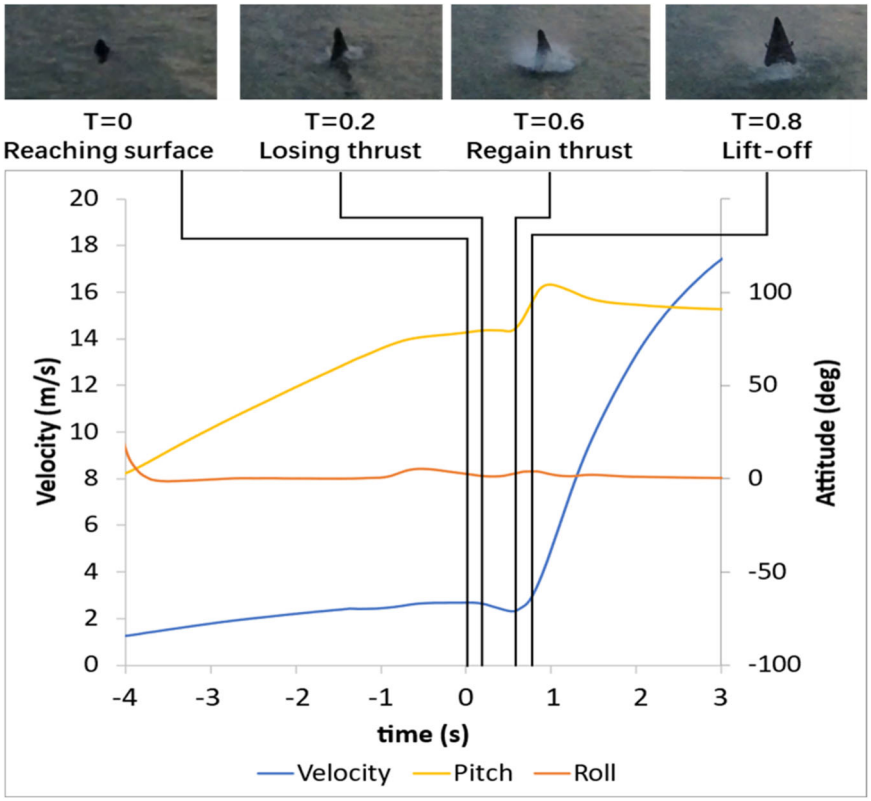

Figure 14 shows the breakdown of the fast water exit. The nose cone reached the water surface at $t = 0$, with a velocity of 2.66 m/s. The vehicle had a pitch angle of about 80°. The vehicle started decelerating at $t = 0.2$ as the propellers lost thrust when they were close to the surface. The vehicle continues moving upwards with kinetic energies built up underwater. At $t = 0.6$, the propellers picked up enough speed to accelerate the vehicle upwards. The vehicle's pitch overshoots the commanded 90° nose-up, probably due to the

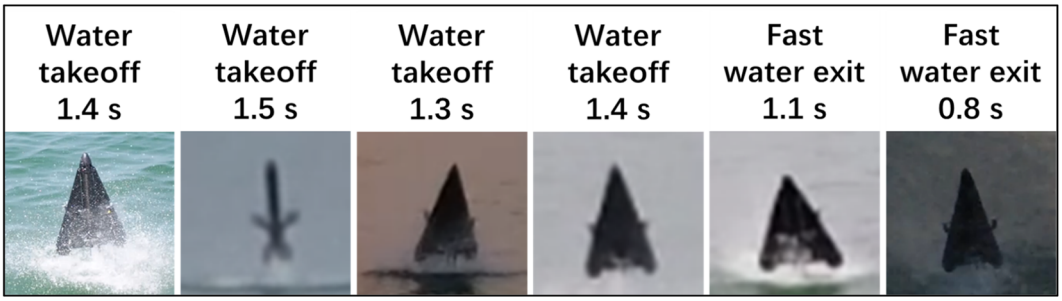

FIGURE 15 Evidence for water-exit repeatability.

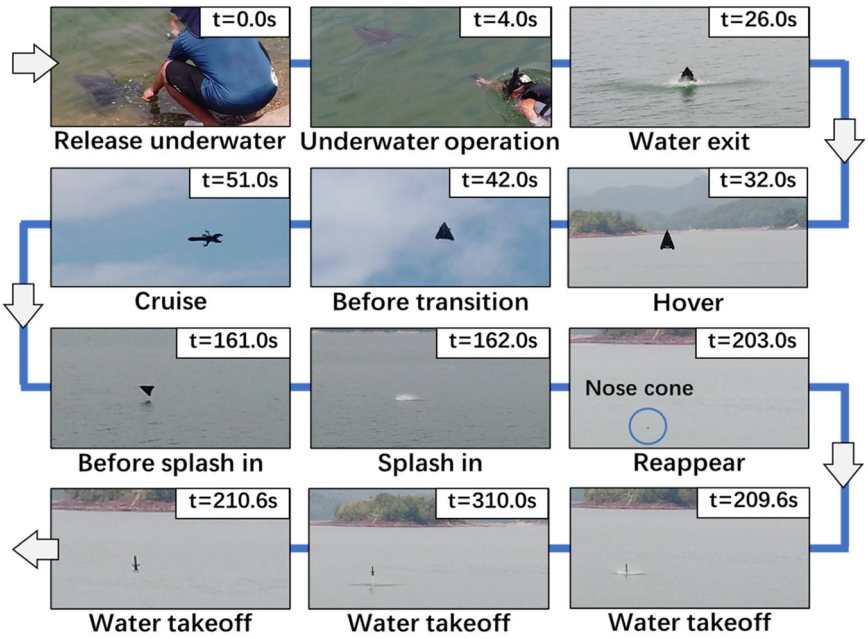

FIGURE 16 Simulated cross-domain mission.

integral term built up in the PID controller when the vehicle does not have enough thrust to respond to pitch control commands. The vehicle cleared the water surface at $t = 0.8$, accelerated rapidly, and the pitch angle returned to 90° nose-up in 2.5 s. The experiment shows that the vehicle can perform a fast water exit with a velocity lower than our predicted 4.77 m/s. This may be due to overestimated drag during water exit and underestimated thrust when propellers cross the surface.

To prove the repeatability of water-to-air transit, we recorded 6 video footages of Nezha-SeaDart performing water-exiting maneuvers during the last day of our field test. As shown in Figure 15. Video evidence is submitted with this article.

5.6 | Mission demonstration

In the simulated mission, the vehicle is released underwater from a dock. It traveled 20 s underwater, pitched 90° and performed a fast water exit. The pilot took over the control with a remote controller when the vehicle was in the air and flew the vehicle to the splash-in point in fixed-wing mode. On arrival at the splash-in point, the vehicle is controlled to perform a fast water entry and stays underwater for about 40 s. It then took off from the water's surface after floating on the surface for 5 s. Footage of the simulated mission is shown in Figure 16.

6 | CONCLUSION

6.1 | Conclusion

The Nezha-SeaDart, as a tail-sitting VTOL fixed-wing HAUV, successfully demonstrated its ability to perform a full aerial-underwater mission. With its VTOL capability, the vehicle can take off and land vertically from ground and water surfaces, reaching a maximum vertical climb rate of 18 m/s. With its fixed-wing cruise capability, the vehicle can travel in the air at a maximum velocity of 35 m/s. The maximum underwater velocity reached by the vehicle was 3 m/s. The vehicle also showed robustness by surviving several unexpected water and ground impacts. The success of

Nezha-SeaDart indicates the possibility of further improving HAUVs' performance by better integrating aerial and underwater systems.

6.2 | Future improvements

Though the Nezha-SeaDart shows the capability of performing full cross-domain missions. It still requires human operation in the air and does not have underwater navigation capability. Its underwater velocity and efficiency are also limited due to the direct use of aerial motors and propellers underwater. The future development of the Nezha-SeaDart should include developing a more automated control system, integrating underwater navigation technologies, and creating a more efficient fluid dynamic profile, propulsion systems and wings. With the method presented in this article, it is possible to estimate and optimize the vehicle's performance at the early stages of the design. However, the assumptions and estimations determined that it would be inaccurate. Better modeling of the vehicle will be needed, especially the modeling of water-exit maneuvers and propeller performance when crossing the water surface.

ACKNOWLEDGMENTS

The authors thank Mr. Hongfei Xie, Mr. Yuling Bai, and Mr. Yuanbo Bi for their help during the manufacturing and testing of Nezha-SeaDart. This research is supported in part by the Science and Technology Commission of Shanghai Municipality Project 20dz1206600, and in part by the Natural Science Foundation of Shanghai under Grant 20ZR1424800, and partly by the Oceanic Interdisciplinary Program of Shanghai Jiao Tong University under Grant SL2022ZD106, SL2023ZD206.

DATA AVAILABILITY STATEMENT

The data that support the findings of this study are available from the corresponding author upon reasonable request.

ORCID

Yufei Jin http://orcid.org/0000-0002-2357-8038

REFERENCES

Alzu'bi, H., Mansour, I. & Rawashdeh, O. (2018) Loon Copter: implementation of a hybrid unmanned aquatic–aerial quadcopter with active buoyancy control. *Journal of Field Robotics*, 35(5), 764–778. Available from: https://doi.org/10.1002/rob.21777

Bi, Y., Jin, Y., Lyu, C., Zeng, Z. & Lian, L. (2022) Nezha-Mini: design and locomotion of a miniature low-cost hybrid aerial underwater vehicle. *IEEE Robotics and Automation Letters*, 7(3), 6669–6676. Available from: https://doi.org/10.1109/Lra.2022.3176438

Guo, D. (2019). *Modelling and experimental investigations of a bi-modal unmanned underwater/air system*. RMIT University. https://researchrepository.rmit.edu.au/esploro/outputs/graduate/Modelling-and-experimental-investigations-of-a/9921864166401341#file-0

Guo, D., Bacciaglia, A., Simpson, M., Bil, C. & Marzocca, P. (2019) Design and development a bimodal unmanned system. In: *AIAA 2019-2096*. AIAA Scitech 2019 Forum.

Jin, Y., Bi, Y., Lyu, C., Bai, Y., Zeng, Z. & Lian, L. (2024) Nezha-IV: a hybrid aerial underwater vehicle in real ocean environments. *Journal of Field Robotics*, 41, 420–442. Available from: https://doi.org/10.1002/rob.22274

Lu, D., Xiong, C., Zhou, H., Lyu, C., Hu, R., Yu, C. et al. (2021) Design, fabrication, and characterization of a multimodal hybrid aerial underwater vehicle. *Ocean Engineering*, 219, 108324. Available from: https://doi.org/10.1016/j.oceaneng.2020.108324

Lu, D., Xiong, C.K., Lyu, B.Z., Zeng, Z. & Lian, L. (2018) Multi-mode hybrid aerial underwater vehicle with extended endurance. In: *2018 Oceans −Mts/IEEE Kobe Techno-Oceans (Oto), Kobe, Japan*. pp. 1–7. https://doi.org/10.1109/OCEANSKOBE.2018.8559438

Lu, D., Xiong, C.K., Zeng, Z. & Lian, L. (2019) A multimodal aerial underwater vehicle with extended endurance and capabilities. In: *2019 International Conference on Robotics and Automation (ICRA)*, pp. 4674–4680. Retrieved from <Go to ISI>: //WOS:000494942303055.

Lyu, C., Lu, D., Xiong, C., Hu, R., Jin, Y., Wang, J. et al. (2022) Toward a gliding hybrid aerial underwater vehicle: design, fabrication, and experiments. *Journal of Field Robotics*, 39(5), 543–556. Available from: https://doi.org/10.1002/rob.22063

Moore, J., Fein, A. & Setzler, W. (2018) Design and analysis of a fixed-wing unmanned aerial–aquatic vehicle. In: *Proceedings of the 2018 IEEE International Conference on Robotics and Automation (ICRA), Brisbane, QLD, Australia*. pp. 1236–1243. https://doi.org/10.1109/ICRA.2018.8461240

Rockenbauer, F.M., Jeger, S., Beltran, L., Berger, M., Harms, M. & Kaufmann, N. et al. (2021) Dipper: a dynamically transitioning aerial–aquatic unmanned vehicle. Paper presented at the Robotics: Science and Systems.

Sareh, S., Siddall, R., Alhinai, T. & Kovac, M. (2017) Bio-inspired soft aerial robots: adaptive morphology for high-performance flight. *Soft Robotics: Trends, Applications and Challenges*, 17, 65–74. Available from: https://doi.org/10.1007/978-3-319-46460-2_9

Siddall, R., Kennedy, G. & Kovac, M. (2018) High-power propulsion strategies for aquatic take-off in robotics. *Robotics Research*, 1(2), 4–19. Available from: https://doi.org/10.1007/978-3-319-51532-8_1

Siddall, R. & Kovac, M. (2015) A water jet thruster for an aquatic micro air vehicle. In: *2015 IEEE International Conference on Robotics and Automation (ICRA), Seattle, WA, USA*. pp. 3979–3985. https://doi.org/10.1109/ICRA.2015.7139755

Siddall, R., Ortega Ancel, A. & Kovač, M. (2017) Wind and water tunnel testing of a morphing aquatic micro air vehicle. *Interface Focus*, 7(1), 20160085. Available from: https://doi.org/10.1098/rsfs.2016.0085

Stewart, W., Weisler, W., MacLeod, M., Powers, T., Defreitas, A., Gritter, R. et al. (2018) Design and demonstration of a seabird-inspired fixed-wing hybrid UAV–UUV system. *Bioinspiration & Biomimetics*, 13(5), 056013. Available from: https://doi.org/10.1088/1748-3190/aad48b

Sun, X., Cao, J., Li, Y. & Wang, B. (2023) Design and field test of a foldable wing unmanned aerial–underwater vehicle. *Journal of Field Robotics*, 41(2), 347–373. Available from: https://doi.org/10.1002/rob.22265

Tan, Y.H. & Chen, B. (2020) A morphable aerial–aquatic quadrotor with coupled symmetric thrust vectoring. In: *2020 IEEE International Conference on Robotics and Automation (ICRA), Paris, France*. pp. 2223–2229. https://doi.org/10.1109/ICRA40945.2020.9196687

Tan, Y.H., Siddall, R. & Kovac, M. (2017) Efficient aerial–aquatic locomotion with a single propulsion system. *IEEE Robotics and Automation Letters*, 2(3), 1304–1311. Available from: https://doi.org/10.1109/Lra.2017.2665689

Weisler, W., Stewart, W., Anderson, M.B., Peters, K.J., Gopalarathnam, A. & Bryant, M. (2018) Testing and characterization of a fixed wing cross-domain unmanned vehicle operating in aerial and underwater environments. *IEEE Journal of Oceanic Engineering*, 43(4), 969–982. Available from: https://doi.org/10.1109/Joe.2017.2742798

Yao, G., Li, Y., Zhang, H., Jiang, Y., Wang, T., Sun, F. et al. (2023) Review of hybrid aquatic–aerial vehicle (HAAV): classifications, current status, applications, challenges and technology perspectives. *Progress in*

Aerospace Sciences, 139, 100902. Available from: https://doi.org/10.1016/j.paerosci.2023.100902

Yao, G., Liang, J., Wang, T., Yang, X., Liu, M. & Zhang, Y. (2014) Submersible unmanned flying boat: design and experiment. Paper presented at the 2014 IEEE International Conference on Robotics and Biomimetics (ROBIO 2014).

Zeng, Z., Lyu, C., Bi, Y., Jin, Y., Lu, D. & Lian, L. (2022) Review of hybrid aerial underwater vehicle: cross-domain mobility and transitions control. *Ocean Engineering*, 248, 110840. Available from: https://doi.org/10.1016/j.oceaneng.2022.110840

Zufferey, R., Ancel, A.O., Farinha, A., Siddall, R., Armanini, S.F., Nasr, M. et al. (2019) Consecutive aquatic jump-gliding with water-reactive fuel. *Science Robotics*, 4(34), eaax7330. Available from: https://doi.org/10.1126/scirobotics.aax7330

SUPPORTING INFORMATION

Additional supporting information can be found online in the Supporting Information section at the end of this article.

How to cite this article: Jin, Y., Zeng, Z. & Lian, L. (2025) Nezha-SeaDart: A tail-sitting fixed-wing vertical takeoff and landing hybrid aerial underwater vehicle. *Journal of Field Robotics*, 42, 137–152. https://doi.org/10.1002/rob.22399